Influence of inflow discharge and bed erodibility on

LU Xue-qiang^{1,2} https://orcid.org/0000-0002-8457-1657; e-mail: luxueqiang18@mails.ucas.ac.cn

* Corresponding author

outburst flood of landslide dam

Citation: Zhou MJ, Zhou GD, Cui KFE, et al. (2019) Influence of inflow discharge and bed erodibility on outburst flood of landslide dam. Journal of Mountain Science 16(4). https://doi.org/10.1007/s11629-018-5312-8

© Science Press, Institute of Mountain Hazards and Environment, CAS and Springer-Verlag GmbH Germany, part of Springer Nature 2019

Abstract: Accurate prediction of the hydrographs of outburst floods induced by landslide dam overtopping failure is necessary for hazard prevention and mitigation. In this study, flume model tests on the breaching of landslide dams were conducted. Unconsolidated soil materials with wide grain size distributions were used to construct the dam. The effects of different upstream inflow discharges and downstream bed soil erosion on the outburst peak discharge were investigated. Experimental results reveal that the whole hydrodynamic process of landslide dam breaching can be divided into three stages as defined by clear inflection points and peak discharges. The larger the inflow discharge, the shorter the time it takes to reach the peak discharge, and the larger the outburst flood peak discharge. The scale of the outburst floods was found to be amplified by the presence of an erodible bed located downstream of the landslide dam. This amplification decreases with the increase of upstream inflow. In addition, the results show that the existence of an erodible bed increases the density of the outburst flow, increasing its probability of transforming from a

Received: 26-Nov-2018 Revised: 15-Jan-2019 Accepted: 17-Feb-2019 sediment flow to a debris flow.

Keywords: Landslide dam; Inflow discharge; Erodible bed; Outburst flood

Notations

A	the intersection point of downstream dam crest
В	the intersection point of upstream dam crest
$B_{\rm c}$	width of dam crest
d_{16} , d_{50} , d_{84}	grain sizes; subscript indicates percent smaller
e	void ratio
g	acceleration due to gravity
H_{d}	height of landslide dam
h_e	height of erodible bed
H_r	height of water level
$H_{\mathbf{w}}$	height of water above final breach bottom
h_0	the depth of dam notch
PE	potential energy of reservoir
$Q_{ m in}$	the upstream inflow discharge
$Q_{ m out}$	the outburst flood discharge
$Q_{ m p}$	the outburst peak discharge
ť	time
t_0	the initial time of dam breaching

¹ Key Laboratory of Mountain Hazards and Earth Surface Process / Institute of Mountain Hazards and Environment, Chinese Academy of Sciences, Chengdu 610041, China

² University of Chinese Academy of Sciences, Beijing 100049, China

$t_{ m p}$	time to peak discharge from the initiation of
ор	dam failure
V_{l}	volume of dammed lake
$V_{\rm d}$	volume of landslide dam
$V_{\rm w}$	volume of water above the final breach
W_0	the width of dam notch
$W_{\rm d}$	width of landslide dam
α	coefficient for dam erodibility
β	rate of change of outburst discharge
β_1, β_2	rate of change of outburst discharge in
ρ_1, ρ_2	Stage 1, Stage 2 respectively
σ	dimensionless measure of the spread in the
$\sigma_{ m g}$	grain-size
θ	angle of large flume
$ heta_1$	angle of upstream dam toe
$ heta_2$	angle of downstream dam toe
$\Delta Q_{ m i}$	relative dimensionless discharge
20	the dimensionless density of outburst
η	floods
$ ho_{ m d}$	the density of debris flow
$ ho_{ m f}$	the density of outburst flood
$ ho_{ m s}$	unit weight of solid material
φ	friction angle of solid materials

Introduction

Landslide dams are natural occurrences which commonly form when river channels are blocked by debris from mass earth movements (Costa and Schuster 1988; Casagli et al. 2003). The primary failure mechanism is overtopping (Korup 2004) since a large-scale landslide dam is often made of loose, easily erodible materials. On the event of an outburst, these granular materials are entrained by the overtopping flood, leading to a downstream sediment flow or even debris flows (Schuster 2000). Sediment-laden outburst floods lead to much greater damage compared to clear water floods. They can bury downstream infrastructures for days or months compared to the brief inundation which results from artificial concrete dam failures. For example, the landslide dam on the Bairaman River of Papua New Guinea, which broke in 1986, released a debris flow flood with an estimated water volume of 4×10^7 m³ and 8×10^7 m³ of rock and soil debris (King et al. 1989). On 8th August 2010, a large-scale debris flow event was triggered by a cascade of landslide dam failures upstream of Zhougu County, China (Cui et al. 2013; Zhou et al. 2013). The debris flow thrust through the urban area and destroyed all buildings along its flow path. The residual deposit flooded half of the urban area

for over 20 days. Therefore, a clear understanding of the changes in the hydrographs of landslide dam overtopping failures and the flow properties of the induced outburst floods is certainly necessary for disaster prevention and mitigation.

Over the past decades, extensive efforts have been made to predict the peak discharge during dam failure. Some of the existing empirical equations (which are widely used in dam overtopping failures) are summarized in Table 1. Previous researches have already found that the peak discharge of outburst floods is a function of dam geometry (dam height, H_d) and dammed lake parameters (water level, H_{r} ; lake volume, V_1) (Kirkpatrick 1977; Singh and Snorrason 1984; Costa 1985; Webby 1996; Pierce et al. 2010). Walder and O'Connor (1997) proposed statistical models where the peak discharge was related to the volume of water released and the drop in the lake water level. However, they also asserted that such relations, even when cast into a dimensionless form, are of limited utility because they fail to portray the effect of breaching process. Peng and Zhang (2012) took a step further when they considered the erodibility of the dam to the failure process. In their statistical model, a parameter α was used to classify landslide dams according to their erodibility (i.e. high, medium, low). They ignored the influence of inflow discharge because of lack of data. However, there are several documented cases where the upstream inflow significantly influenced the breaching process and the resulting flooding (Capart 2013). An example would be the temporary landslide dam that formed in Hsiaolin, Taiwan, during the typhoon Morakot (Dong et al. 2011; Li et al. 2011). Since the landslide occurred during a record-breaking flood, the inflow into the lake was relatively high compared to the breach outflow and consequently resulted to a mega flood (i.e., measured peak discharge equaled to 27,060 m³/s) (cf. Li et al. 2011). This flood was several times larger than that of previously recorded outburst floods induced by large-scale landslide dam failures (cf. 6500 m3/s of the Tangjiashan Landslide dam reported by Liu et al. (2009) and Ning et al. (2010)). However, the specific correlation between the upstream inflow and the outburst flood remains unclear. This is primarily due to the lack of data obtained under well controlled conditions and/or from real

Table 1 Empirical equations for calculation of the peak discharge (Q_p)

Empirical expression	Empirical calculation (m ³ /s)	Parameter	Reference
$Q_{\rm p} = 1.268(H_{\rm w} + 0.3)^{2.5}$	1.268	$H_{\rm w}$: height of water above final breach bottom (m)	Kirkpatrick (1977)
$Q_{\rm p} = 13.4 (H_{\rm d})^{1.89}$	6.829	H _d : dam height (m)	Singh and
$Q_{\rm p} = 1.776(V_{\rm l})^{0.47}$	1.434	V_1 : volume of dammed lake (m ³)	Snorrason (1984)
$Q_{\rm p} = 1.154 (V_{\rm w} H_{\rm w})^{0.412}$	0.826	$V_{\rm w}$: volume of water above the final breach (m ³) $H_{\rm w}$: height of water above final breach bottom (m)	MacDonald and Langridge Monopolis (1984)
$Q_{\rm p} = 0.763 (V_{\rm l} H_{\rm w})^{0.42}$	0.543	V ₁ : volume of dammed lake (m ³) H _w : height of water above final breach bottom (m)	Costa (1985)
$Q_{\rm p} = 0.063 PE^{0.42}$	~	PE: potential energy of water	Costa and Schuster (1988)
$Q_{\rm p} = 0.607 V_{\rm w}^{0.295} H_{\rm w}^{1.24}$	0.341	$V_{\rm w}$: volume of water above the final breach (m ³) $H_{\rm w}$: height of water above final breach bottom (m)	Froehlich (1995b)
$Q_{\rm p} = 0.0443 g^{0.5} V_{\rm l}^{0.367} H_{\rm w}^{1.40}$	0.071	g : is the acceleration of gravity (m/s²) V_1 : volume of dammed lake (m³) H_w : height of water above final breach bottom (m)	Webby (1996)
$Q_{\rm p} = 0.0176 (V_{\rm w} H_{\rm w})^{0.606}$	0.011	V_w: volume of water above the final breach (m³)H_w: height of water above final breach bottom (m)	Pierce et al. (2010)
$Q_{\rm p} = g^{\frac{1}{2}} H_d^{\frac{5}{2}} \left(\frac{H_{\rm d}}{H_{\rm r}}\right)^{-1.371} \times \left(\frac{V_{\rm l}^{1/3}}{H_{\rm d}}\right)^{1.536} e^a$	1.204	$H_{\rm d}$: dam height (m) g : is the acceleration of gravity (m/s²) $H_{\rm r}$: height of water level (m) $V_{\rm l}$: volume of dammed lake (m³) a : coefficient for dam erodibility	Peng and Zhang (2012)
$Q_{\rm p}=(H_{\rm w})^{2.5}$	0.410	$H_{\rm w}$: height of water above final breach bottom (m)	Hakimzadeh et al.
$Q_{\rm p} = 0.6971 (H_{\rm w})^{1.5} (V_{\rm l})^{0.25}$	0.364	$H_{\rm w}$: height of water above final breach bottom (m) V_1 : volume of dammed lake (m ³)	(2014)

Notes: The measured outburst peak discharges downstream the non-erodible and erodible beds ranged from 0.0149 to 0.0173 m³/s and from 0.0167 to 0.0277 m³/s, respectively.

measurements.

Another important factor which can strongly affect the hydrograph of outburst floods is the loose deposits (erodible bed) behind the landslide dam. After the river is blocked by a landslide dam, the downstream area behind the dam quickly dries up, exposing the loose sediment deposits on the river bed (Costa and Schuster 1988; Casagli et al. 2003; Korup 2004). During the dam failure process, these deposits are easily eroded and entrained by the outburst flood. Previous experimental tests, which evaluated the crucial factors that influence the peak discharge, (e.g., Coleman et al. 2002; Cao et al. 2011; Xu et al. 2013; Walder et al. 2015) did not consider bed erosion. It has been shown however (Bellos et al. 1992) that the loose deposits behind landslide dams actually serve as a rough contact surface to the outburst flooding (Wu 2007, 2013). This rough bed dissipates the kinetic energy of the water flow, effectively providing resistance to the flow motion. On the other hand, the entrained

loose granular materials increase the flood's potential energy, improving the mobility of the solid-water two-phase flow (Fannin and Wise 2001; Wang et al. 2003; Breien et al. 2008). Although, benchtop experiments have recently demonstrated that bed-sediment entrainment by dry granular avalanches can, in some cases, be accompanied by increased flow-front speeds and farther run-out distances (Mangeney et al. 2007) they have limited relevance to sediment flows (Iverson 1997, 2010). Therefore, it is still unclear how the erodible bed affects the outburst floods that result from landslide dam overtopping failures.

This paper presents a series of flume model tests that are aimed to study the effects of different boundary conditions on outburst floods due to landslide dam overtopping failure. Three different upstream inflow discharges $(2.0 \times 10^{-3}, 3.0 \times 10^{-3}, 5.3 \times 10^{-3} \, \text{m}^3/\text{s})$ as well as two different downstream sloping bed conditions (i.e., erodible and nonerodible bed) were considered in the physical tests.

These experiments were designed to: (i) investigate the effects of different upstream inflows and channel bed conditions on the hydrographs of outburst floods especially on the peak discharge, and (ii) study the changes in the densities of outburst flows during the dam failure process to evaluate the effects of bed erodibility on the subsequent flow properties. Seepage failure and piping are not considered in the tests since they are seldom found in real cases (Peng and Zhang 2012). To reduce the effects of seepage or piping on the dam failure process, the water in the reservoir was allowed to fill rapidly.

1 Experimental Setup

1.1 Model design

Scaling laws play a crucial role in designing physical model tests which aim to understand the behavior of geomorphological phenomena involving grain-fluid mixtures (Iverson et al. 2015). This includes experimental tests on landslide dam overtopping failures (Costa and Schuster 1988; Korup 2004). After a series of dimensional analyses, Peng and Zhang (2012) proposed a set of dimensionless numbers $\frac{H_d}{W_d}$, $\frac{V_d^{1/3}}{H_d}$, and $\frac{V_l^{1/3}}{H_d}$ that can be used to define the geometrical characteristics of landslide dams and dammed lakes. The ratio of the dam height to its width $\left(\frac{H_d}{W_d}\right)$ defines the slope erosion and controls the velocity of water flow and the pertinent erosion rate. The ratio between the cubic root of the dam volume and height, also known as the dam shape coefficient $\left(\frac{V_{\rm d}^{1/3}}{H_{\rm d}}\right)$, reflects the amount of granular material that can be entrained and can influence the breaching duration. The lake shape coefficient $\left(\frac{V_1^{1/3}}{H_d}\right)$ is the ratio between the cube root of the water volume and the dam height. It indicates the potential volume of water that can be poured out to erode the dam, thus influencing the breach size and the outflow discharge. To verify if the experimental dam can represent real large-scale landslide dams, its dimensionless coefficients were evaluated against those of 80 reported landslide dams from different

locations around the world, which were formed from rock avalanches, debris flows, and other types of geophysical mass flows (see Figure 1a). As shown in Figure 1a the symmetry of the data points, where each one represents a single natural landslide dam, plotted in log-linear coordinates is remarkable. This indicates a positive correlation between the volume of the dam body and the volume of the dammed lake. This positive linear relationship was also presented by Korup (2004) (Figure 1b). Moreover, the data points are mainly distributed in two symmetric bands. The points which fall in these bands can represent typical landslide dams. The dimensionless coefficients that define the modeled landslide dam presented in this paper fall within the concentrated area and can therefore be considered to represent real landslide dams.

1.2 Experiment setup

experimental landslide Six dams constructed in a large flume near DDFORS (Dongchuan Debris Flow Observation Research Station), Dongchuan District, Yunnan Province, China (N26°14', E103°08'). The flume is basically a straight concrete channel (45 m long, 0.7 m wide and 1.4 m deep), inclined at 12° to the horizontal (Figure 2a) (Zhou et al. 2015). This flume angle, along with the dammed lake shape and depth, is used to calculate the dammed lake volume V_1 . The relatively large flume angle results to a representative point (Star in Figure 1) which is relatively low. This relatively large angle more closely resembles that of a mountain gully, where debris flow more easily. At the lower end of the flume, the slope opens up to a horizontal concrete plane. The flume walls and run-out area are made up of smooth cement. Along the walls of the flume are five 1 m wide reinforced glass windows, which allow the observation of the dam overtopping process (Figure 2a). A water container, with a capacity of 12 m³, was connected to the top of the flume through a channel with rows of saw-teeth, which dissipates any turbulent energy from the released upstream flow, effectively minimizing the turbulence effects experienced by the dam downstream. A section of the large flume (10 m long), with two glass windows, was selected for this landslide dam overtopping failure test (Figure 2b).

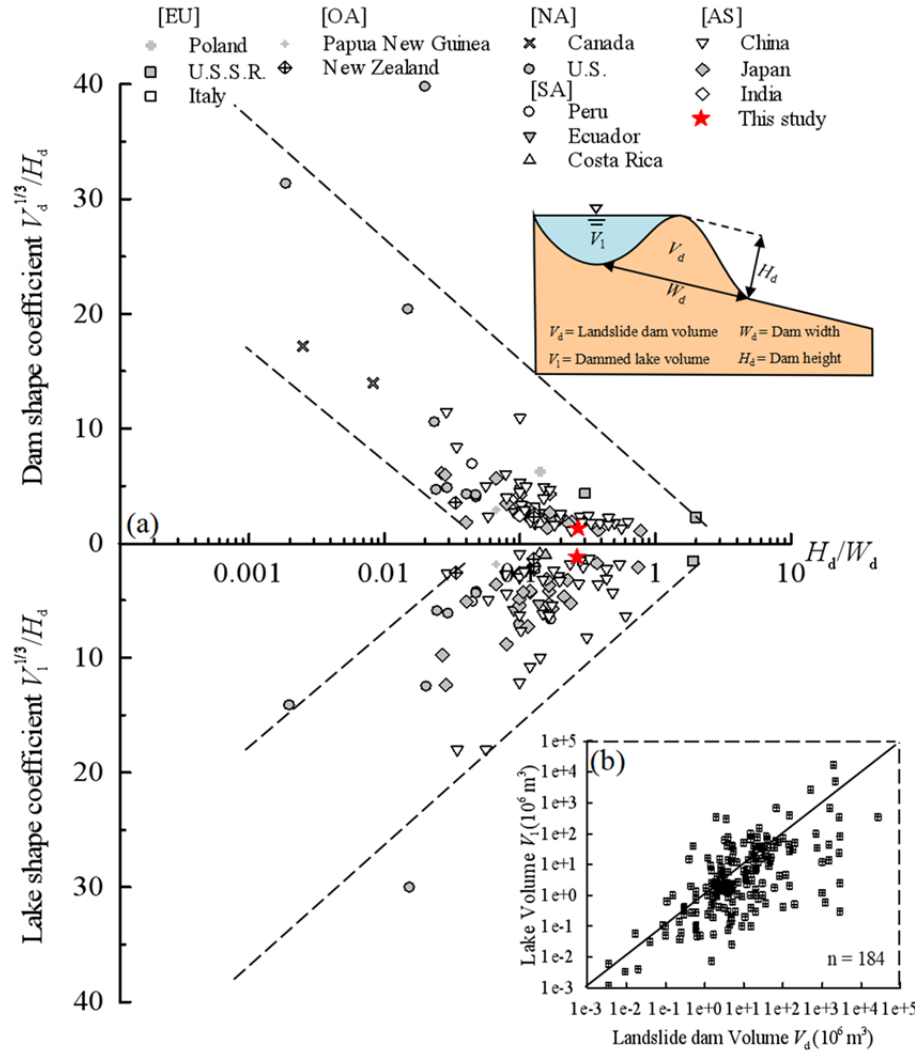


Figure 1 (a) Ternary plot of landslide-dam dimensionless parameter derived from a worldwide data set (Costa and Schuster 1988; Korup 2004; Xu et al. 2009; Yin et al. 2009; Peng and Zhang 2012); (b) The relationship between landslide dam volume and lake volume (Korup, 2004). ([NA] is North America, [SA] is South America, [EU] is Europe, [OA] is Australia, and [AS] is Asia).

The modeled landslide dams were built upstream of the glass window (Figure 2b). The geometry of the dam is trapezoidal and is fixed in all tests. Another downstream glass window, with a height of 0.4 m, is converted into a side wall of the flume. This makes it convenient for continuous sampling during the tests (Figure 2b). The distance between the downstream dam toe and a certain data collection area is 5 m. For the experimental tests which involve erodible beds, this region is filled with loose sediment 0.2 m thick (Figure 2b).

Dam construction proceeded as follows: granular materials were well-mixed and poured from the same height onto the sloping channel to form landslide dams that were in accordance with the natural repose angle of soils. Manual compaction was adopted to ensure that the void ratio $(0.78 \sim 0.80)$ each layer was consistent with field conditions which were usually in the range of 0.59 ~ 1.11 (cf. Chang and Zhang 2010; Chang et al. 2011). This process was repeated until the desired dam geometry was achieved. The same material, construction process and void ratio were employed for the erodible bed. After dam crest was smoothed and leveled, a rectangular notch ($h_0 \times$ w_0 =0.05 m × 0.1 m) was excavated on the dam crest, adjacent to the glass sidewall (Figure 2b). This ensures that the overtopping failure starts at the same place every time, guaranteeing the repeatability ofthe experiments. Moreover, this method of symmetry analysis is convenient for the observation of the failure process, and can be

used for studying the outburst floods as demonstrated by Hakimzade et al. (2014).

To capture the evolution of the landslide dams and outburst floods, three digital video cameras (SONY FDR-AX40, 1440×1080 pixels, 25 fps) and one laser sensor (Leuze, ODSL 30/V-30M-S12) with a resolution of ±1 mm were installed above the channel. One digital video camera (camera1) was positioned on the free side of the glass panel (Figure 3), and was set to capture the longitudinal evolution process of the landslide dam. Another camera (camera 2) was used to complement the process obtained by camera 1. Camera 3 was installed to calculate the velocity of the outburst

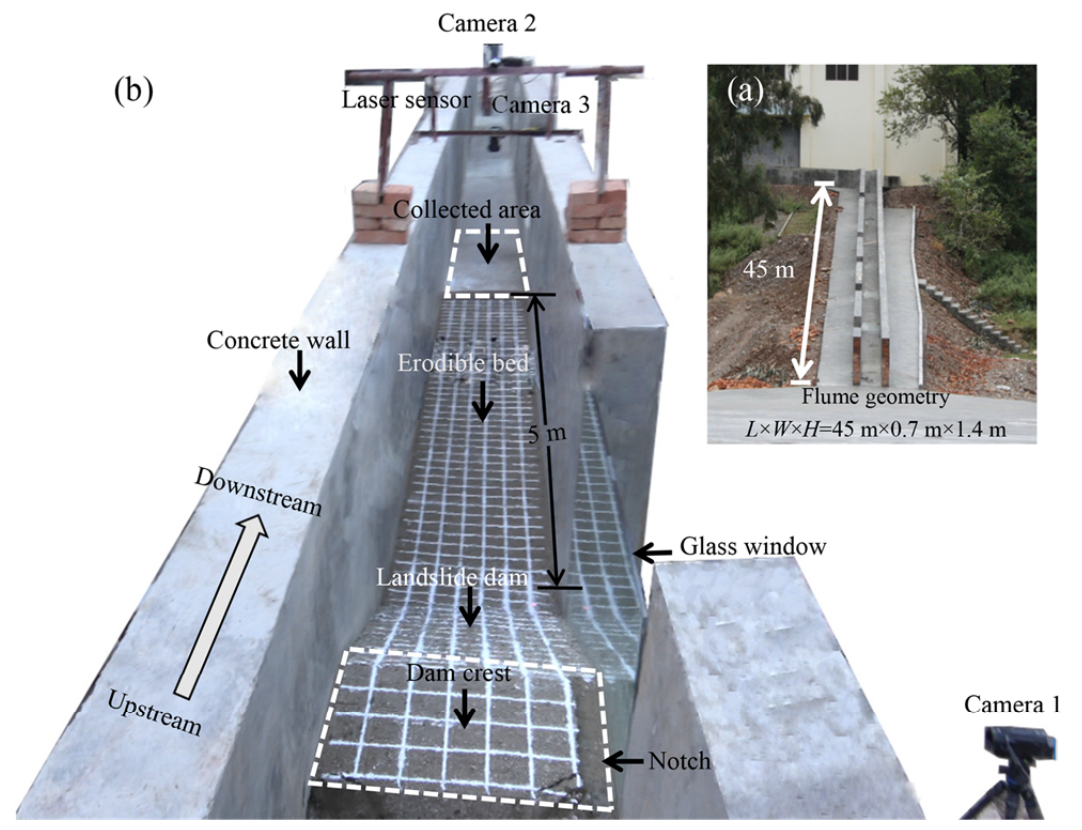


Figure 2 (a) A large debris flow flume in DDFORS (45 m long, 0.7 m wide and 1.4 m deep, inclined at 12° to the horizontal); (b) A front view of the model dam as viewed from the upstream region of the flume. The dam, which is built on a concrete floor, is confined by walls 0.7 m apart and 1.4 m high. In erodible bed tests, a 0.2 m thick, 5 m long flat pile is connected to the dam toe.

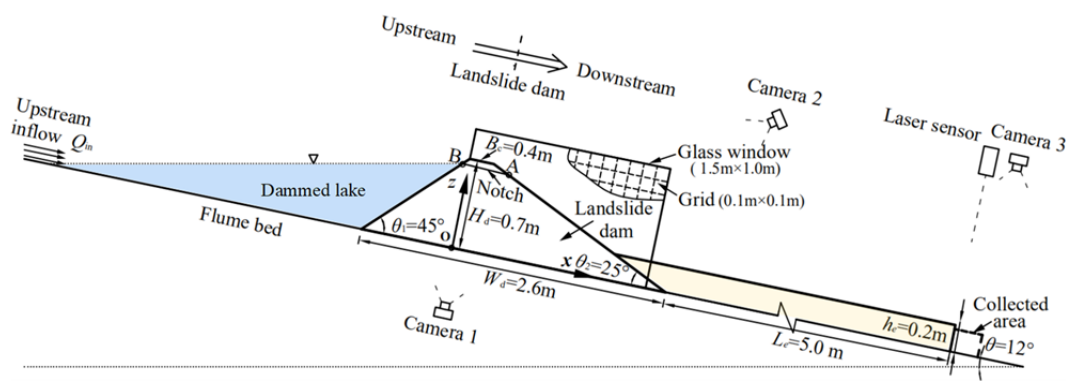


Figure 3 Schematic diagram of the model dam with the exact dimensions. The reservoir depth is maximum at the dam and tapers to zeros upstream.

flooding through the motion of tracer particles as they travel further downstream. The laser sensor was used to measure the depth of the outflow (Gregoretti et al. 2010; Pickert et al. 2011). By combining the data from the laser sensor and the videos from camera 3, the outburst discharge can be measured at the collection area, 5 m downstream of the dam toe (Figure 3). In addition,

manual continuous sampling was adopted during the tests to calculate the changes of the outburst flood density.

1.3 Granular material

The geotechnical behavior of landslide dams (e.g., shear strength) and the dam failure processes are closely correlated to the grain size distribution

of the granular materials (cf. Swanson et al. 1986; Casagli et al. 2003). To emulate the poorly-sorted soils of natural landslide dams, the granular materials in the Jiangjia Ravine near DDFORS were used. Figure 4 shows the cumulative grain size distribution interval of 42 landslide dams in the Northern Apennines (cf. Casagli et al. 2003) and the grain-size distribution of the modeled landslide dams. The diameters of fine particles (which have passed through a 0.25 mm sieve) were measured using a Malvern Mastersizer 2000 instrument. This device is designed to measure the sizes of small particles within a sample and the corresponding size distribution based on the laser diffraction principle and on known particle size distribution statistics (Malvern Instruments Ltd 2007). Considering the grain size effect, the particles with diameters larger than 20 mm were removed in all tests. As such, the impact of big boulders on the dam evolution process and outburst hydrograph is not considered in this study. Sediment samples experiment sets had mean grain diameters of d_{50} = 0.85 mm. The spread

of the grain-size distribution within the constructed dams was obtained to be, $\sigma_{\rm g} = \frac{d_{84}}{d_{16}} = 75$ (Walder 2016) indicating a wide grain size range. As shown in Figure 4, the grain size distributions of the experimental dams fall within the range of distributions (indicated by the shaded region) observed in natural landslide dams, such as those in the Northern Apennines (Casagli et al. 2003). Therefore, the material used in this study can represent real landslide dams, especially for those largely composed of fine particles. The unit weight and friction angle of the solid materials were measured to be $\rho_{\rm s} = 2650~{\rm kg/m^3}$ and $\varphi = 30^{\circ}$,

1.4 Experimental procedure

respectively (cf. Zhou and Ng 2010).

After dam construction, all the instruments were simultaneously switched on. The water valve was opened and the upstream flow entered the dammed lake. As the water started to flow over the dam crest, tracer particles were dropped to capture the landslide dam failure process and to estimate the velocity of the outburst flood. When the

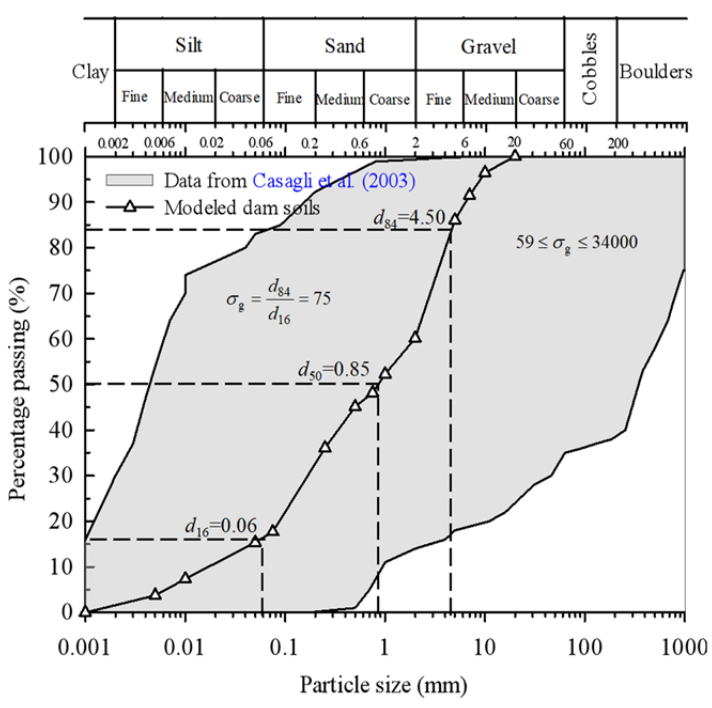


Figure 4 The shaded region is the cumulative grain size distribution of 42 landslide dams in the Northern Apennines (cf. Casagli et al. 2003), and the solid line represents the grain-size distribution of the modeled landslide dams. A mean size of $d_{50} = 0.85$ mm and dimensionless measure of the spread in the grain-size distribution $\sigma_g = 75$ was adopted in all experimental set-ups.

outburst flood first arrives at the collection area, the manual sampling begins. Sixteen samples were taken for each experiment covering the whole process of dam overtopping failure.

Two sets of tests were conducted to investigate the effect of the inflow discharge and the presence of an erodible bed downstream on the outburst floods. A test in each set corresponded to a single inflow discharge which was set to be 2.0×10⁻³, 3.0×10⁻³, and 5.3×10⁻³ m³/s. The first set (Test Nos. N-Q2.0, N-Q3.0, and N-Q5.3) served as a control set-up where no erodible bed was installed. In the second set (Test Nos. E-Q2.0, E-Q3.0 and E-Q5.3), the erodible bed was installed according to the specifications prescribed in the previous section. Details of the modeling tests are summarized in Table 2.

2 Results

2.1 General observations

2.1.1 Evolution process of dam breaching

Table 2 Test program and results

	Test ID	Upstream inflow Q_{in} (×10 ⁻³ m ³ /s)	Void ratio e	Time to peak discharge t_p (s)		Rate of outburst discharge β_1	Rate of outburst discharge β_2
Non-	N-Q2.0	2.0	0.81	97	14.9	0.05	0.32
erodible	N-Q3.0	3.0	0.79	91	15.5	0.01	0.25
bed	N-Q5.3	5.3	0.82	54	17.3	0.02	0.40
Erodible	E-Q2.0	2.0	0.81	127	16.7	0.01	0.71
bed	E-Q3.0	3.0	0.79	96	19.5	0.04	0.21
beu	E-Q5.3	5.3	0.82	48	27.7	0.20	0.34

Notes: $\beta_1 = \frac{\Delta Q_1}{\Delta t}$ Rate of outburst discharge in Stage 1. $\beta_2 = \frac{\Delta Q_2}{\Delta t}$ Rate of outburst discharge in Stage 2.

In the test with erodible bed behind landslide dam, the erodible bed material used is the same as that of the dam material, and the void ratio is nearly 0.8. In the test without erodible bed, the dam is directly connected with the cement floor.

The rapid change of the hydrodynamic conditions during landslide dam breach makes the process of dam failure very complex. The initial time of dam breaching $t_0 = 0$ s (Test No. N-Q5.3) begins when water starts to travel along the initial notch and eventually reaches the downstream crest, Point A (Figures $5a_1$ and $5a_2$). This is where the overtopping failure of landslide dams initially occur.

At first stage, the hydrodynamic conditions are still insufficient to erode the soils. The overtopping flow depth is still shallow and the flow velocity is still quite small. As such, most of the sediment transport is still confined to the area immediately below dam crest Point A (Figures 5b₁ and 5b₂). Most of the eroded material, at this point, do not yet travel very far and are simply deposited at the nearest point downstream (Figure 5b1), advancing as an alluvial fan that moves towards the toe of the dam (Figure 5b2). This alluvial fan formation and increase of the particle concentration in the flow during the initiation of landslide dam overtopping failure was also observed by Walder et al. (2015). As the upstream inflow continues to supply flowing water, the hydrodynamic power gradually increases and so does the erosion rate. Outburst floods start develop, further entraining the soil and increasing the amount of suspended particles in the water. By this point, the inflowing water erodes some parts of the upstream crest bounded by Points A and B (Figures 5c₁ -5d₂). Viewing the process from the side and the front, one can observe the formation of step-pools (cf. Zhou et al. 2015) (Figures $5c_1$ - $5d_2$). In this stage, the entire dominated by the continuous development of the rectangular breach, while the sides remain relatively stable. This is a type of head-cut erosion stage.

When the erosion point reaches Point B at t_4 = 43 s (Figures 5e₁ and 5e₂), the dam crest completely collapses and the water level of the dammed lake quickly decreases as larger amounts of water are released downstream. The geometry of the sloping bed begins to smoothen out (Figure 5e₁) as a result of its exposure to the rapid water flows, indicating the end of head-cut erosion stage. At this point, the failure of the side slopes and the rest of the dam begin (Figure 5e₂). This further accelerates the erosion process along the dam surface. The water flow at the overtopped dam crest is clear. However, it becomes murky and sediment-laden near the dam toe as it entrains soil particles along its path. At the time t_5 = 51 s, the depth of the water starts to decline (Figure 5f₁), and the side slope failure continues (Figure 5f₂) until the water level in the reservoir is close to the residual dam height (Figures $5g_1$ - $5h_2$). At this point, no further erosion occurs.

2.1.2 Hydrological evolution of outburst floods

Figure 6 shows the outburst flood of a single landslide dam overtopping failure process without any erodible bed installed. The initial time (t = 0 s) is kept along the same timeline as with the breach evolution process. No discharge was measured before the time at which the flow front first reaches the collection area downstream (Figure 6a). The first discharge was measured at t = 32 s, marking the arrival of the initial surges. At t = 47 s, an inflection point – a sudden positive change in the discharge trend – is observed, marking the occurrence of outburst flooding. This rapid rise in the discharge profile ends when the peak discharge

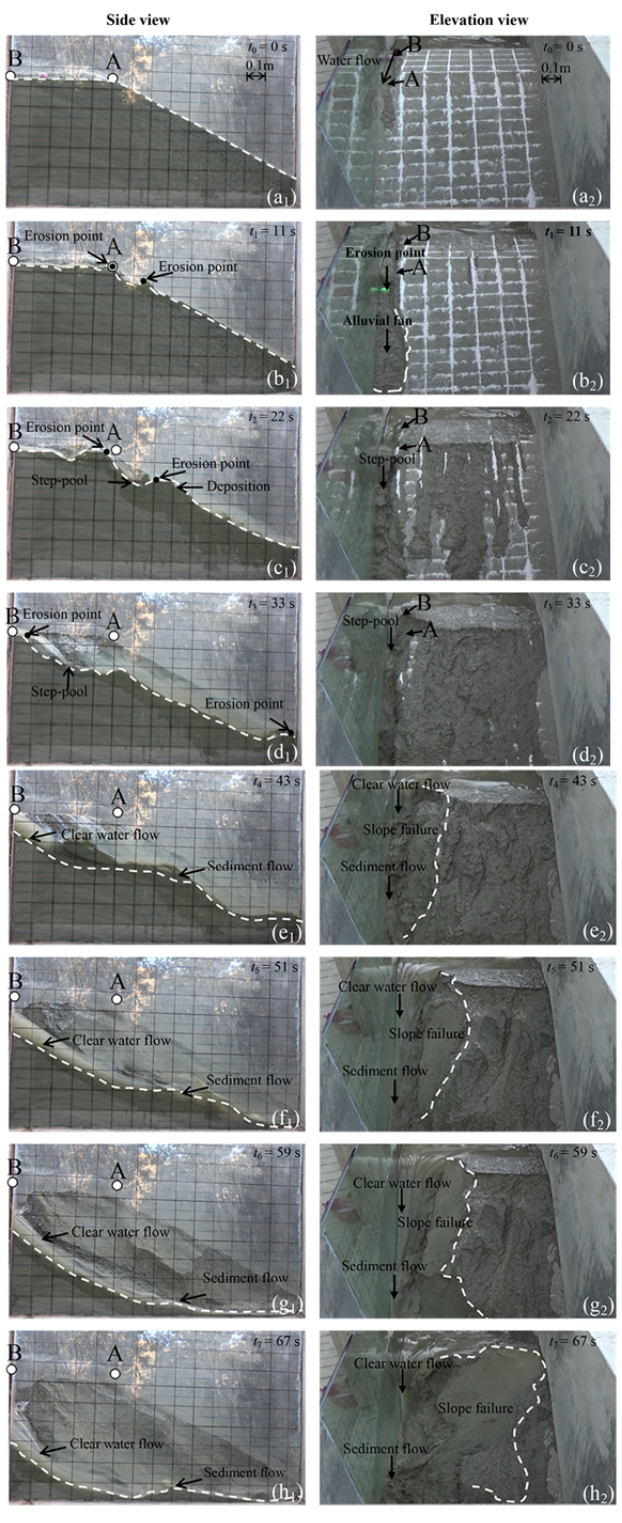


Figure 5 Snapshots of the dam-breaching process (Test No. N-Q5.3). $t_0 = 0$ s is the moment when water starts to travel along the initial notch and eventually reaches the downstream crest. The size of a single grid on the viewing window and lime grid is 0.1 m \times 0.1 m. The dashed lines mark the surface profile of the dam geometry in side vies and elevation view.

is achieved, which is about 7 seconds after the inflection point. Thereafter, the outburst floods attenuate while maintaining a relatively large discharge over a longer period of time compared to the flows before the inflection point. Approaching the end of the experiment, as the outburst floods weaken, the measured discharges gradually decrease, asymptotically approaching the value $\frac{Q_{\rm out}}{Q_{\rm in}}=1$. At t=80 s, the erosion and dam failure stops.

The density of the floods corresponding to the sampled outburst floods were measured (Figure 6b). Although the flood density fluctuates in Figure 6b, the trend is basically a steady decrease. During the early stages of the dam failure, the flood density is relatively high, indicating the formation of debris flows (Figure 6b area 'A'). The outburst flow is unstable mainly due to the irregular collapses of soils that occur along the longitudinal direction due to head-cut e rosion. At the end of the head-cut erosion stage, the fluctuation of the flow density eases. The transition to the lower densities

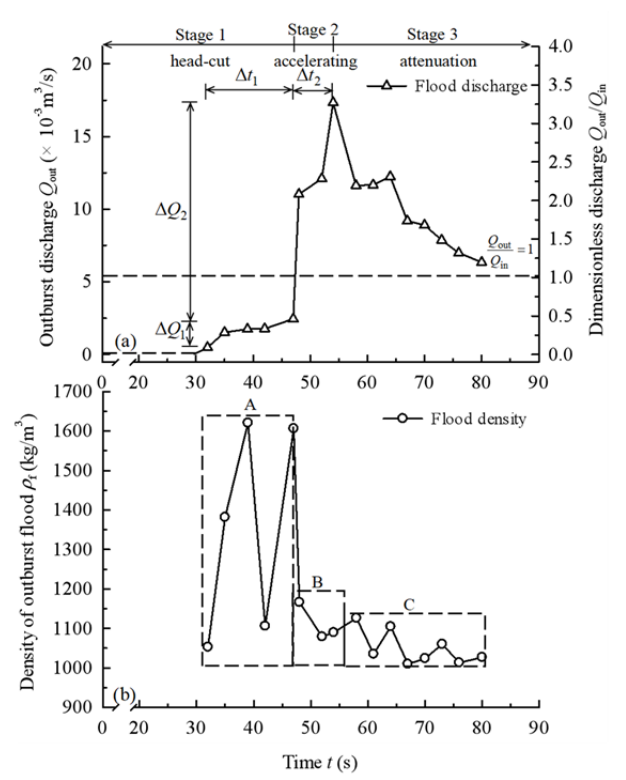


Figure 6 Time t = 0 s marks the moment when water starts to travel along the initial notch and eventually reaches the downstream crest. (a) Hydrograph for dambreach experiment reported in this paper (Test No. N-Q5.3); (b) The water density of outburst floods.

corresponds to the time at which the peak discharges were recorded, at around t=54 s. The outburst floods in this stage are mostly sediment flows with densities ranging from 1100 kg/m³ to 1200 kg/m³ (Figure 6b area 'B'). After t=54 s, the densities of the outburst floods are further reduced to a range of 1000 kg/m³ to 1100 kg/m³ (Figure 6b area 'C') . Erosion stops at the end of the dam failure, and the flow gradually changes to clear water (same as the upstream inflow) with a density of about 1000 kg/m³

2.1.3 Three stages of dam breaching

Comparing the hydrographs in Figure 6 with the cross-sectional evolution of the overtopping failure in Figures 5e₁ and 5e₂, one can find that the inflection point (at t = 47 s) roughly coincides with the time at which the erosion point reaches the upstream dam crest, whereupon the dam crest was totally eroded (at t_4 = 43 s). In addition, there is a coincidence between the amount of erosion observed at $t_5 = 51$ s (Figure $5f_1$) and the peak discharge of the outburst flood at t = 54 s, as measured downstream (Figure 6a). Note that the minor time difference is due to the delay at which initial discharge can be measured, owing to the distance between the dam itself and the data collection area. This relationship indicates that the inflection point physically corresponds to the time when the dam crest was totally eroded which resulted in outburst flooding. The results can be explained by the broad-crest weir equation relationship (Singh and Scarlatos 1988; Coleman et al. 1997) which assumes that the amount of discharge increases with the increase of the relative height between the water level in the dammed lake and the dam crest. Therefore, the failure process is actually closely related to the outburst flood.

From the hydrograph and longitudinal surface profiles, three distinct stages of dam failure can be defined. The rate of change of the outburst discharge can be used to help explain the three-stage division:

$$\beta = \frac{\Delta Q_{\rm i}}{\Delta t} \tag{1}$$

where β is the rate of change of outburst discharge, ΔQ_i is the relative dimensionless discharge ($\Delta \frac{Q_{\text{out}}}{Q_{\text{in}}}$), and Δt is the change in time. Stage 1 is termed as the 'head-cut erosion process'. This stage starts when the first erosion point moves from the

downstream dam crest at Point A to the upstream dam crest at Point B. The pertinent outburst discharge increases from zero to the inflection discharge (Figure 6a). During this stage, both the value of the outburst discharge and the rate of change are small ($\beta_1 = 0.02$). During Stage 2, the erosion process starts to 'accelerate'. After the erosion point reaches the upstream dam crest (at Point B), the depth and the downstream velocity of the water flow rapidly increases. This causes the outflow discharge to rapidly increase ($\beta_2 = 0.4$) until the peak discharge is reached. During Stage 3, the erosion 'attenuates'. The water flow depth and the outflow discharge start to decrease, and the landslide dam undergoes rapid failure. Eventually, the outflow discharge equalizes with the value of the upstream inflow $\left(\frac{Q_{\text{out}}}{Q_{\text{in}}}=1\right)$. Comparing the rates of change of the outburst flow discharge during Stage 1 (β_1) and Stage 2 (β_2), it can be seen that $\beta_1 \ll \beta_2$ in all tests (see Table 2). This further illustrates that before the water erosion point approaches the upstream crest Point B, the outflow discharge is small $\left(\frac{Q_{\text{out}}}{Q_{\text{in}}} < 1\right)$, and so is the rate of outflow discharge change β . However, once the soil at the upstream dam crest (Point B) has been completely eroded, the discharge rate of outburst flooding will also rapidly increase. It is noted, that this behavior is found to be independent of the presence of an erodible bed (see Table 2), and will occur with or without it. Such a clear turning point serves as a good criterion for the identification of the two different stages (Stages 1 and 2), which can be used as a guideline for providing early warnings for landslide dam outburst peak flow.

2.2 Influence of upstream inflow discharge on the downstream outburst floods

Figure 7 shows the hydrograph of outburst floods induced by landslide dam overtopping with non-erodible beds behind the dam. From Figure 7a, one can observe that all the outburst floods under different upstream inflows undergo three stages: erosion, accelerating erosion attenuating erosion. The first flow that arrives at the collection area is strongly affected by the inflow discharge. The larger the inflow discharge (Q_{in}) , the shorter the time needed for it to reach the downstream collection area, causing hydrograph to draw closer to the Y axis. In addition, the larger the inflow discharge (Q_{in}) , the shorter the time to achieve the peak discharge. It also follows that the larger the inflow, the larger the peak discharge (Q_p). However, this linear

relationship between peak discharge and inflow discharge, as shown in Figure 7a, was found to be quite weak. To further illustrate the effects of inflow discharge on the outburst flood, the dimensionless discharge $\frac{Q_{\text{out}}}{Q_{\text{in}}}$ was once again

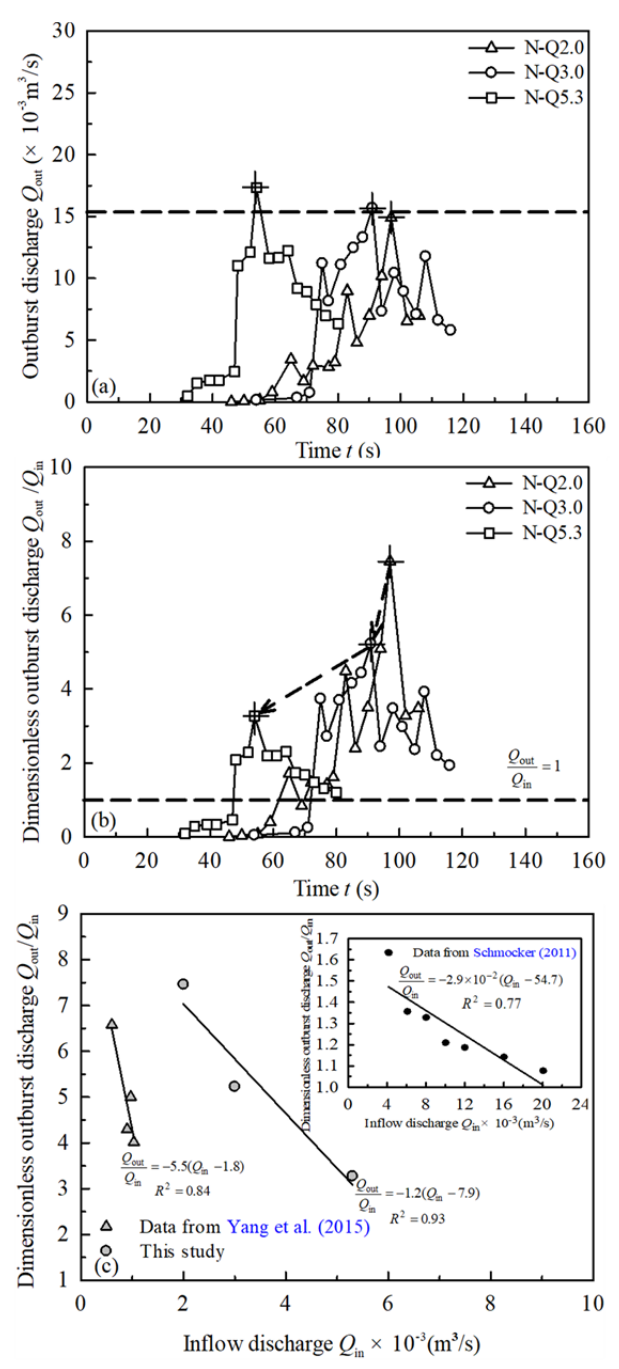


Figure 7 Flow amplification effect of landslide dams on outburst flood. (a) Hydrograph for dam-breach tests with non-erodible beds (Test Nos. N-Q2.0, N-Q3.0, N-Q5.3); (b) Measured flood amplification with time. (c) The relationship between inflow discharge $(Q_{\rm in})$ and the amplification of peak discharge $(\frac{Q_{\rm p}}{Q_{\rm in}})$.

adopted (Figure 7b). $\frac{Q_{\text{out}}}{Q_{\text{in}}}$ <1, means that the landslide dam can reduce the water flow, $\frac{Q_{\text{out}}}{Q_{\text{out}}} = 1$ means landslide dam has no effect on water flow, $\frac{Q_{\text{out}}}{}$ >1 means that the landslide dam can amplify the discharge. In Stage 1, the dams retain the water from the upstream flow reg ardless of its magnitude ($\frac{Q_{\text{out}}}{Q_{\text{in}}}$ <1). Once the first stage finishes, the upstream inflow is rapidly amplified due to the rapid failure of landslide dam. At this stage, the dimensionless discharge $(\frac{Q_{\text{out}}}{Q_{\text{in}}})$ can no longer be less than one. It is interesting to note that the smaller the upstream inflow rate (2.0×10⁻³, 3.0×10⁻³, 5.3×10⁻³ m³/s), the larger the amplification effect (7.5, 5.2, 3.3) (Figure 7b). When the previous experimental results (e.g., Schmocker 2011; Yang et al. 2015) are reinterpreted, similar results can be observed: the dimensionless peak discharge $\frac{Q_P}{Q_P}$ decrease with the inflow discharge (Figure 7c). This indicates that even in some rivers where the upstream inflow is small, massive downstream flooding can still be expected once a landslide dam is formed. The difference in the regression curves (Figure 7c), in terms of slope and intercept, are mainly due to the differences in dam geometry and material.

2.3 Influence of erodible bed on the downstream outburst floods

Landslide dams are usually formed in mountainous river regions where loose deposits are abundant (Casagli et al. 2003; Korup 2004). In the erodible bed tests (as shown in the Figure 8), similar outburst flood hydrographs can still be observed for the three experiments and the three stages of outburst flooding still exist (Figure 8a). The larger the upstream inflow, the shorter the period of Stage 1 and the more rapid the development of Stage 2. It also follows that, similar to the non-erodible test results, the larger the inflow, the shorter the time to achieve the peak discharge (cf. Table 2). From Figure 8a, one can find that the measured peak flow discharges (0.0149-0.0173 m³/s in non-erodible bed tests and 0.0167- 0.0277 m3/s in erodible bed tests) are within the range as predicted by the empirical formulas in Table 1 regardless of the boundary condition. However, it has to be emphasized that the uncertainty of the empirical formulas are very large, and the prediction range for the same dam

can span several orders of magnitude (Q_p =0.011-6.829 m³/s) (Table 1). The extent of this deviation lies in the fact the regression analysis can only be applied to a certain range. Once it exceeds a certain sampling interval, the accuracy of the prediction decreases.

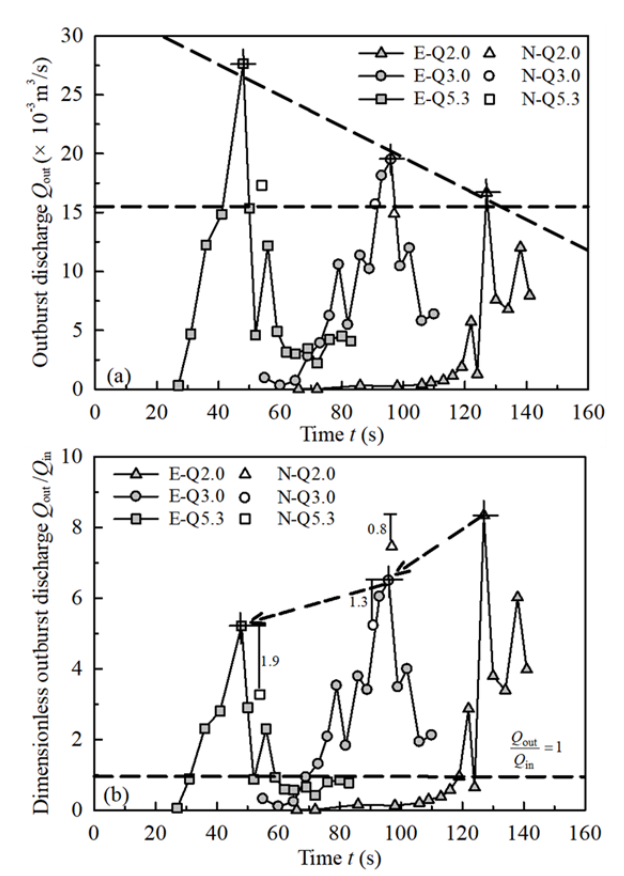


Figure 8 Flow amplification effect of landslide dams on outburst flood. (a) Hydrograph for dam-breach tests with erodible beds (Test Nos. E-Q2.0, E-Q3.0, E-Q5.3); (b) Measured flood amplification with time.

The primary difference between the two cases is that the peak discharges are larger when an erodible bed is present (cf. Figure 8a). In addition, compared to the non-erodible bed test results, which are distributed in a horizontal line, the peak discharge points in erodible bed tests are distributed along a steep line (Figure 8a). This indicates that the peak discharges of outburst floods, which further entrain erodible beds, are strongly influenced by upstream inflows. This is very different from the findings of previous non-erodible bed experiments that confirm the upstream inflow has little effect on the peak flow discharge (Cao et al. 2011; Xu et al. 2013). The

upstream inflow can significantly, not only decrease the time to peak discharge, but also magnify the flood discharge.

It was also observed that the dimensionless peak discharges (i.e., 8.3, 6.5, 5.2) decrease as upstream inflow increases, similar to that of the non-erodible tests (Figure 8b). The dimensionless outburst discharges are further amplified due to the presence of an erodible bed. As the inflow discharge is increased, the differences between the dimensionless discharges of the erodible and non-erodible bed cases also increase (Figure 8b: 0.8, 1.3, 1.9). Therefore, once the erodible bed exists behind the dam, the influence of upstream inflow on the peak flow discharge becomes more evident. This means that the erodible bed is a crucial element in the landslide dam with non-trivial effects to the development of outburst floods.

2.4 Evolution of outburst flood density

Landslide dam outburst floods may be either sediment flows or debris flows. Figure 9 shows the effect of the upstream inflow on the density of the outburst floods. Solid markers represent the cases with erodible beds while the hollow ones are for those with non-erodible beds. All data points from different test configurations (i.e. inflow discharge, erodible bed, non-erodible bed) fell between 1000-1680 kg/m³. In order to highlight the differences in the fluid properties, and to show whether outburst floods can indeed become hyperconcentrated flows or even debris flows, a dimensionless density for

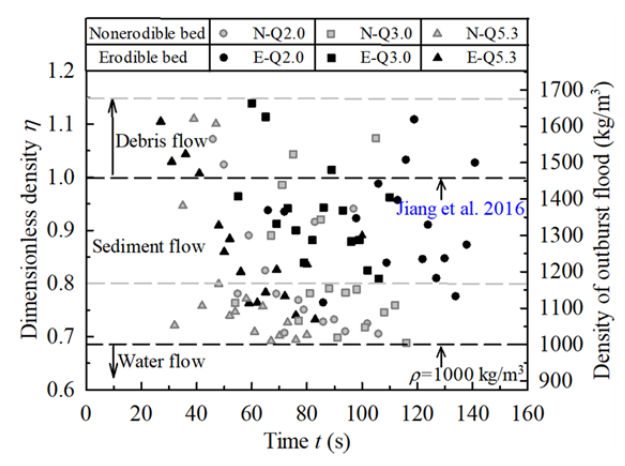


Figure 9 Dimensionless densities computed from all flume test cases.

outburst floods is proposed:

$$\eta = \frac{\rho_{\rm f}}{\rho_{\rm d}} \tag{2}$$

where ρ_f is the density of outburst floods, and ρ_d is a representative density of debris flow. Here $\rho_{\rm d} = 1460 \text{ kg/m}^3 \text{ was adopted (cf. Jiang et al.}$ **2016**). An η that is greater than 1 implies that a debris flow is formed; while η that is less than 1 but larger than 0.68 implies that the flood is a sediment flow. It is noted that the points are mainly concentrated in areas where η is greater than 0.68 and less than 1, which implies that outburst floods, for most cases, are sediment flows. Debris flows ($\eta=1$) can be formed regardless of the bed conditions (i.e., erodible or not). Although the debris flows can occur in the landslide dam failure process, the results presented here may also be strongly affected by the inclination of the flume used in the tests. According to the experimental study of landslide dam overtopping failure, Jiang et al. (2016) demonstrated that the unit weight of the water/sand mixture increases as the bed slope increases within the range of 2°-13°. The erodible bed behind the dam has little effect on the maximum density of the outburst flood ($\eta=1.15$) during the overtopping failure Furthermore, one can find that the probability of debris flows forming is higher in the erodible tests (21%) than in the non-erodible bed tests (13%). In addition, one can observe that most of the nonerodible bed test points mainly congregate below 0.8, especially near the density of clean water at 0.68. This is in contrast to the points in the erodible bed group which concentrate above 0.8. These results illustrate that loose deposits behind the dam can increase the density of the flow, making it easier for the outburst flood to change from clear water flow to sediment-laden flow and then to debris flows. Therefore, the erodible bed behind the dam can make the outburst flood carry more granular mass, significantly increasing its impact on the downstream areas.

3 Conclusions

By flume model tests, the effects of upstream inflow discharge and downstream bed erodibility on outburst flooding induced by landslide dam overtopping failure were investigated. The key conclusions are drawn as follows:

- (1) According to the hydrograph of the downstream outburst flood, three stages of the dam breach evolution can be identified. Once the upstream dam crest is eroded by the water flow, an inflection occurs in the hydrograph, marking the occurrence of an outburst discharge. The outflow discharge then rapidly increases until a peak is achieved. Such a phenomena provides an appropriate criterion for the early warning of landslide dam outburst peak flow.
- (2) The larger the inflow, the shorter the time it takes to reach the peak discharge. In addition, the dependence of peak discharge on inflow discharge is stronger when an erodible bed exists behind the dam. The opposite is true if no erodible bed is present.
- (3) The larger the upstream inflow, the smaller the scale amplification of the outburst floods. This trend is more pronounced in erodible bed tests. The dimensionless outburst discharges are much larger due to the presence of an erodible bed. As the inflow discharge is increased, the difference of the dimensionless discharges between the erodible and non-erodible bed cases also increases.
- (4) Landslide dam outburst floods are, most of the time, sediment flows though debris flows may be observed. The existence of an erodible bed behind the landslide dam can increase the density of the outburst flood, and increase its possibility of transforming from a sediment flow to debris flows. The density of outburst flows if an erodible bed is present is usually greater than 1168 kg/m³ (0.8 in dimensionless form).

The failure process of a landslide dam is a process which involves complicated geotechnical and hydro-dynamic concepts. By using dimensionless parameter analysis, we were able to account for most of the geometrical features that would define a natural landslide dam. Despite this, the constructed model dam still suffers from several limitations. For example, the relatively large flume angle we adopted closely resembles that of a mountain gully instead of river bed, where mobile debris flow more easily. Meanwhile the steeper the angle of the flume, the higher is the kinetic energy of the inflowing water (converted from potential energy) (cf. Jiang et al. 2016) which may further influence the consequent dynamics of the outburst flood. This will be the focus of our

future work, along with the consideration of the slope angle effect on the outburst flow dynamics,

erosion evolution of landslide dam, and its outburst floods.

Acknowledgments

The authors acknowledge the financial support from the National Natural Science Foundation of China (Grant No. 41731283), the Key Research Program of Frontier Sciences, Chinese Academy of Sciences (CAS) (Grant No. QYZDB-SSW-DQC010), and the Youth Innovation Promotion Association, Chinese Academy of Sciences (CAS).

References

Bellos CV, Soulis V, Sakkas JG (1992) Experimental investigation of two-dimensional dam-break induced flows. Journal of Hydraulic Research 30(1): 47-63.

https://doi.org/10.1080/00221689209498946

Breien H, De Blasio FV, Elverhøi A, et al. (2008) Erosion and morphology of a debris flow caused by a glacial lake outburst flood, Western Norway. Landslides 5: 271-280. https://doi.org/10.1007/s10346-008-0118-3

Cao Z, Yue Z, Pender G, (2011) Landslide dam failure and flood hydraulics. Part I: experimental investigation. Natural Hazards 59(2): 1003-1019.

https://doi.org/10.1007/s11069-011-9814-8 Capart H (2013) Analytical solutions for gradual dam breaching and downstream river flooding. Water Resources Research 49(4): 1968-1987. https://doi.org/10.1002/wrcr.20167

Casagli N, Ermini L, Rosati G (2003) Determining grain size distribution of material composing landslide dams in the Northern Apennine: sampling and processing methods. Engineering Geology 69(1): 83-97.

https://doi.org/10.1016/s0013-7952(02)00249-1

Chang DS, Zhang LM (2010) Simulation of the erosion process of landslide dams due to overtopping considering variations in soil erodibility along depth. Natural Hazards & Earth System Sciences 10(4): 933-946.

https://doi.org/10.5194/nhess-10-933-2010 Chang DS, Zhang LM, Xu Y, et al. (2011) Field testing of erodibility of two landslide dams triggered by the 12 may wenchuan earthquake. Landslides 8(3): 321-332.

https://doi.org/10.1007/s10346-011-0256-x

Coleman SE, Andrews DP, Webby MG (2002) Overtopping Breaching of Noncohesive Homogeneous Embankments. Journal of Hydraulic Engineering 128(9): 829-838.

https://doi.org/10.1061/(asce)0733-9429(2002)128:9(829) Coleman SE, Jack RC, Melville BW (1997) Overtopping breaching of noncohesive embankment dams. Proc., 27th Congress of the Int. Association for Hydraulic Research, San Francisco, pp 42-47.

Costa JE (1985) Floods from Dam Failures. U.S. Geological Survey, Open-File Report No. 85-560.

Costa JE, Schuster RL (1988) The formation and failure of natural dam. Geological Society of America Bulletin 100: 1054-1068.

Cui P, Zhou GGD, Zhu XH et al. (2013) Scale amplification of natural debris flows caused by cascading landslide dam failures. Geomorphology 182(427): 173-189.

https://doi.org/10.1016/j.geomorph.2012.11.009 Dong JJ, Li YS, Kuo CY, et al. (2011) The formation and breaching of a shortlived landslide dam at Hsiaolin village, Taiwan-Part I: Post-event reconstruction of dam geometry. Engineering Geology 123: 40-59.

https://doi.org/10.1016/j.enggeo.2011.04.001

Fannin RJ, Wise MP (2001) An empirical-statistical model for debris flow travel distance. Canadian Geotechnical Journal 38(5): 982-994. https://doi.org/10.1139/t01-030

Froehlich DC (1995b) Peak Outflow from Embankment Dam. Journal of Water Resources Planning &Management 121(1): 90-97.

https://doi.org/10.1061/(asce)0733-9496(1995)121:1(90)

Gregoretti C, Maltauro A, Lanzoni S (2010) Laboratory experiments on the failure of coarse homogeneous sediment natural dams on a sloping bed. Journal of Hydraulic Engineering 136(11): 868-879.

https://doi.org/10.1061/(asce)hy.1943-7900.0000259

Hakimzadeh H, Nourani V, Amini AB (2014) Genetic programming simulation of dam breach hydrograph and peak outflow discharge. Journal of Hydrologic Engineering 19(4):

https://doi.org/10.1061/(asce)he.1943-5584.0000849

Iverson RM (2015) Scaling and design of landslide and debrisflow experiments. Geomorphology 244: 9-20.

https://doi.org/10.1016/j.geomorph.2015.02.033
Iverson RM, Reid ME, LaHusen RG (1997) Debris-flow mobilization from landslides. Annual Review of Earth and Planetary Sciences 25: 85-138.

https://doi.org/10.1146/annurev.earth.25.1.85

Iverson RM, Reid ME, Logan M, et al. (2010) Positive feedback and momentum growth during debris-flow entrainment of wet bed sediment. Nature Geoscience 4(2): 116-121. https://doi.org/10.1038/ngeo1040

Jiang X, Cui P, Chen H, et al. (2016) Formation conditions of outburst debris flow triggered by overtopped natural dam failure. Landslides 14(3): 1-11.

https://doi.org/10.1007/s10346-016-0751-1

King J, Loveday I, Schuster RL (1989) The 1985 Bairaman landslide dam and resulting debris flow, Papua New Guinea. Quarterly Journal of Engineering Geology and Hydrogeology 22(4): 257-270.

https://doi.org/10.1144/gsl.qjeg.1989.022.04.02
Kirkpatrick GW (1977) Evaluation guidelines for spillway adequacy. Evaluation of Dam Safety. Proceedings of the Engineering Foundation Conference. pp 395-414.

Korup O (2004) Geomorphometric characteristics of New Zealand landslide dams. Engineering Geology 73(1-2): 13-35. https://doi.org/10.1016/j.enggeo.2003.11.003

Li MH, Sung RT, Dong JJ, et al. (2011) The formation and breaching of a short-lived landslide dam at Hsiaolin Village, Taiwan - Part II: Simulation of debris flow with landslide dam breach, Engineering Geology 123: 60-71. https://doi.org/10.1016/j.enggeo.2011.05.002

propagation after the dam break. Science in China 52(4): 801-

Liu N, Zhang JX, Lin W, et al. (2009) Draining Tangjiashan barrier lake after Wenchuan earthquake and the flood 809.

- MacDonald TC, Langridge-Monopolis J (1984) Breaching Characteristics of Dam Failures. Journal of Hydraulic Engineering 110(5): 567-586.
- Malvern Instruments Ltd (2007) MAN0384-1.0 Mastersizer 2000 User Manual.
- Mangeney A, Tsimring LS, Volfson D, et al. (2007) Avalanche mobility induced by the presence of an erodible bed and associated entrainment. Geophysical Research Letters 34(22): 22401. https://doi.org/10.1029/2007gl031348
- Ning L, Chen Z, Zhang JX, et al. (2010) Draining the Tangjiashan barrier lake. Journal of Hydraulic Engineering 136(11): 914-923.
 - https://doi.org/10.1061/(asce)hy.1943-7900.0000241
- Peng M, Zhang LM (2012) Breaching parameters of landslide dams. Landslides 9(1): 13-31.
 - https://doi.org/10.1007/s10346-011-0271-y
- Pierce MW, Thornton CI, Abt SR (2010) Prediction peak outflow from breached embankment dams, Journal of Hydrologic Engineering 15(5): 338-349.
 - https://doi.org/1061/(asce)he.1943-5584.0000197
- Pickert G, Weitbrecht V, Bieberstein A (2011) Breaching of overtopped river embankments controlled by apparent cohesion. Journal of Hydraulic Research 49(2): 143-1561. https://doi.org/10.1080/00221686.2011.552468
- Schmocker L (2011) Hydraulics of dike breaching. PhD thesis, Swiss Federal Institute of Technology.
 - https://doi.org/10.3929/ethz-a-006716949194
- Schuster RL (2000) Outburst debris-flows from failure of natural dams. Proceedings 2nd international conference on debris flow hazard mitigation. pp 16-20.
- Singh KP, Snorrason A (1984) Sensitivity of outflow peaks and flood stages to the selection of dam breach parameters and simulation models. Journal of Hydrology 68(1): 295-310. https://doi.org/10.1016/0022-1694(84)90217-8
- Singh VP, Scarlatos PD (1988) Analysis of gradual earth-dam failure. Journal of Hydraulic Engineering 114 (1): 21-42. https://doi.org/10.1061/(asce)0733-9429(1988)114:1(21)
- Swanson FJ, Oyagi N, Tominaga M (1986) Landslide dam in Japan. In: Schuster, R.L. (Ed.), Landslide Dam: Processes Risk and Mitigation. American Society of Civil Engineers Geotechnical Special Publication 3. pp 131-145.
- Walder JS (2016) Dimensionless erosion laws for cohesive sediment. Journal of Hydraulic Engineering 142(2): 04015047.
 - https://doi.org/10.1061/(asce)hy.1943-7900.0001068
- Walder JS, Iverson RM, Godt JW, et al. (2015) Controls on the breach geometry and flood hydrograph during overtopping of

- noncohesive earthen dams. Water Resources Research 51(8): 6701-6724. https://doi.org/10.1002/2014wr016620
- Walder JS, O'Connor JE (1997) Methods for predicting peak discharge of floods caused by failure of natural and constructed earthen dams. Water Resources Research 33(10): 2337-2348. https://doi.org/10.1029/97wr01616
- Wang G, Sassa K, Fukuoka H (2003) Downslope volume enlargement of a debris slide—debris flow in the 1999 Hiroshima, Japan, rainstorm. Engineering Geology 69(3): 309-330. https://doi.org/10.1016/s0013-7952(02)00289-2
- Webby MG (1996) Discussion of "Peak outflow from breached embankment dam" (Froehlich, 1995b). Journal of water resources Planning and Management 122(4): 316-317.
- Wu WM (2007) Computational river dynamics. Taylor & Francis, Leiden. pp 69-70.
- Wu WM (2013) Simplified Physically Based Model of Earthen Embankment Breaching. Journal of Hydraulic Engineering 139(8): 837-851.
 - https://doi.org/10.1061(asce)hy.1943-7900.0000741
- Xu FG, Yang XG, Zhou JW, et al. (2013) Experimental research on the dam-break mechanisms of the Jiadanwan landslide dam triggered by the Wenchuan earthquake in China. The Scientific World Journal (6): 272363.
 - https://doi.org/10.1155/2013/272363
- Xu Q, Fan XM, Huang RQ, et al. (2009) Landslide dams triggered by the Wenchuan earthquake, Sichuan province, southwest China. Bulletin of Engineering Geology and the Environment 68(3): 373-386.
 - https://doi.org/10.1007/s10064-009-0214-1
- Yang Y, Cao SY, Yang KJ, et al. (2015) Experimental study of breach process of landslide dams by overtopping and its initiation mechanisms. Journal of Hydrodynamics, Ser.B 27(6): 872-883.
 - https://doi.org/10.1016/S1001-6058(15)60550-9
- Yin Y, Wang F, Sun P (2009) Landslide hazards triggered by the 2008 Wenchuan earthquake, Sichuan, China. Landslides 6(2): 139-152. https://doi.org/10.1007/s10346-009-0148-5
- Zhou GGD, Cui P, Chen HY, et al. (2013) Experimental study on cascading landslide dam failures by upstream flows. Landslides 10(5): 633-643.
 - https://doi.org/10.1007/s10346-012-0352-6
- Zhou GGD, Ng CWW (2010) Dimensional analysis of natural debris flows. Canadian Geotechnical Journal 47(7): 719-729. https://doi.org/10.1139/t09-134
- Zhou GGD, Cui P, Tang JB et al. (2015) Experimental study on the triggering mechanisms and kinematic properties of large debris flows in Wenjia gully. Engineering Geology 194: 52-61. https://doi.org/10.1016/j.enggeo.2014.10.021